energies

MDPI

Article

Coherence Effects on the Power and Tower Loads of a 7 × 2 MW Multi-Rotor Wind Turbine System

Shigeo Yoshida [1,*], Uli Goltenbott [2], Yuji Ohya [1] and Peter Jamieson [3]

1 Research Institute for Applied Mechanics, Kyushu University, 6-1 Kasugakoen, Kasuga, Fukuoka 816-8580, Japan; ohya@riam.kyushu-u.ac.jp
2 Department of Aeronautics and Astronautics, Kyushu University, 744 Motooka, Nishi-ku, Fukuoka 819-0395, Japan; uli@riam.kyushu-u.ac.jp
3 Wind Energy Research-Center for Doctoral Training, University of Strathclyde, Royal Collage R336, Glasgow G1 1XW, UK; peter.jamieson@strath.ac.uk
* Correspondence: yoshidas@riam.kyushu-u.ac.jp; Tel.: +81-92-583-7747

Academic Editor: Frede Blaabjerg
Received: 16 June 2016; Accepted: 30 August 2016; Published: 13 September 2016

Abstract: A multi-rotor system (MRS), in which multiple wind turbines are placed on one tower, is a promising concept for super-large wind turbines at over 10 MW due to the cost and weight advantages. The coherence effects on an MRS were investigated in this study. Although a wide range of coherences were measured so far, a decay constant of $C = 12$ is recommended in the IEC61400-1 standard. Dynamic simulations were performed for a 14-MW MRS, which consists of seven 2-MW turbines and includes wind models with three different coherences. Although the results show that a larger coherence increases the output power and the collective loads due to tower base fore-aft bending, it reduces the differential loads due to tower-base torque and tower-top nodding. The most significant case is the fatigue damage due to tower base fore-aft bending, which was more than doubled between the decay constants of $C = 6$ and $C = 12$. The present results indicate that the coherence should be defined carefully in the design of large-scale MRSs because its effect on them is not straightforward.

Keywords: wind turbine; multi-rotor; load; power; coherence

1. Introduction

To achieve higher economic efficiency, commercial wind turbines have grown progressively larger over the past three decades. The rotor diameter and the rated power have reached 200 m and 10 MW, respectively. Furthermore, the research and development of super-large wind turbines higher than the 10-MW class is being promoted in many research organizations in the world.

Most of the wind turbines are single-rotor systems (SRSs), in which one rotor is placed on the tower. Although SRSs are well developed, including design standards, guidelines and design tools, they require the development of extremely large cutting-edge parts, such as blades, bearings and gearboxes, for super large wind turbines. This development sometimes causes problems in supply, cost and delivery. On the contrary, multi-rotor systems (MRSs) are an attractive alternative because they consist of multiple commercial wind turbines (a mature technology), and no large cutting-edge parts are required, except for the support structure and yawing system for MRSs.

The concept of MRSs has a long history over 80 years, and although several prototypes were built, no advantages have been found over conventional SRSs. After a long absence from the industry, MRSs started to draw interest due to their economic advantages.

Concerning small wind turbine projects, the Southwest Research Institute [1] conducted a study on an MRS consisting of seven 400-W wind turbines through wind tunnel tests and computational fluid dynamics (CFD). The aerodynamic mutual interferences of the turbines were shown to cause no loss in output power. However, Goltenbott et al. [2] showed that the aerodynamic interaction contributes to an increase in the output power of MRSs with diffuser-augmented wind turbines. They found that the output power increases up to 9% with respect to the simple summation of single turbines with an optimum separation of the turbines.

Above all, the most extensive research on large-scale MRS concepts was performed by Jamieson [3,4] and in the INNWIND Project [5]. A 20-MW MRS consisting of 45 444-kW wind turbines was defined, and the aerodynamic characteristics of the aerodynamic interference (such as between the rotors), load calculations, research (such as optimization of the support structure) and power wiring are completed. Finally, in comparison with an SRS of 20 MW, the initial cost will increase to 118%, and the power generation cost is expected to decrease to 85%. Verma [6] also studied the cost of 5-MW MRS consisting of three units of 1.66-MW wind turbines. The research shows that the cost of the total system is expected to decrease to 87% of the 5-MW SRS. There is still room for the optimization and discussion of the cost of the MRS, construction, maintenance, and so on, as shown by these previous research works.

The costs of the energy of the MRS consists of n wind turbines with the rotor diameter d and the SRS with the rotor diameter D were compared, assuming the cost is proportional to the mass, the mass is proportional to the cube of the rotor diameter and the energy production is proportional to the square of the rotor diameter. The relative mass of the MRS to the SRS, which have the same total rotor area, is shown by the following equation:

$$\frac{m}{M} = \frac{nkd^3}{kD^3} = \frac{d}{D} = \frac{1}{\sqrt{n}} \tag{1}$$

where k is the constant.

This cost of MRSs is not adequate, as the above relation does not consider the cost of the support structure. Mate [7] designed and estimated the cost of the support structures of two types of 5-MW MRS: three 1.66-MW turbines and seven 0.71-MW turbines. His results show that the cost is decreased in comparison with a 5-MW SRS. For non-structural parts, the cost reductions are 15% and 18%, respectively, for each case, and for the whole MRS, including support structures, 5% and 3%, respectively. Furthermore, MRSs are expected to have a further cost reduction in production. Stronger competition between the vendors of smaller mature parts would lower the cost of these parts. The assembly of MRSs can further decrease the cost, as the smaller parts are easier to handle, and series production would contribute to an efficient assembly.

In addition, the INNWIND Project [5] insisted that MRSs are effective for levelling the loads and the output power due to spatial variation in the wind speed [4]. This is effective to reduce the fatigue loads at the tower base, as well as smoothing power. This is an important suggestion, as the support structure and yawing system are large concerns in the design of MRSs. While the total design load estimation is essential, an estimation of the effects of the design wind conditions have been completed.

Considering the situation above, the effects of the inflow coherence on the energy production and on the tower base fatigue loads were investigated for a 14-MW MRS, which consists of seven units of mature 2-MW wind turbines, through dynamic simulation.

2. Simulation Outlines

2.1. Analysis Method

BLADED (DNV GL, Bristol, UK) [8] was used for the dynamic response analysis of the MRS. It uses a modified blade-element and momentum theory. A modal method combined with multibody dynamics is applied to determine the elasticity of the structures. A wind turbine controller is integrated into the model.

2.2. Wind Turbine Model

An MRS consisting of seven 2-MW wind turbines is defined in this paper. The basic specifications of the MRS are summarized below.

Number of rotor: 7.
Rotor diameter: 80 m.
Rated power: 2 MW.
Number of blades: 3.
Tilt angle: 0°.
Rotor speed: 12–20 min^{-1}.
Cut in-out wind speed: 4–25 m/s.
Blade mass: 6.5 t.
Rotor mass: 33.6 t.
Nacelle mass: 72.0 t.
Flapwise 1st mode frequency: 0.87 Hz.
Edgewise 1st mode frequency: 1.30 Hz.
Flapwise 2nd mode frequency: 2.81 Hz.

The arrangement and positions of each rotor are shown in Table 1 and Figure 1. The number of the centre turbine is #0, and the #1–#6 turbines are arranged counter clockwise around the wind direction. The features of the model are described below.

Table 1. Hub centre positions of the 7 × 2 MW MRS.

#	x(m)	y(m)	z(m)
0	0	0	160
1	0	−40	230
2	0	−80	160
3	0	−40	90
4	0	40	90
5	0	80	160
6	0	40	230

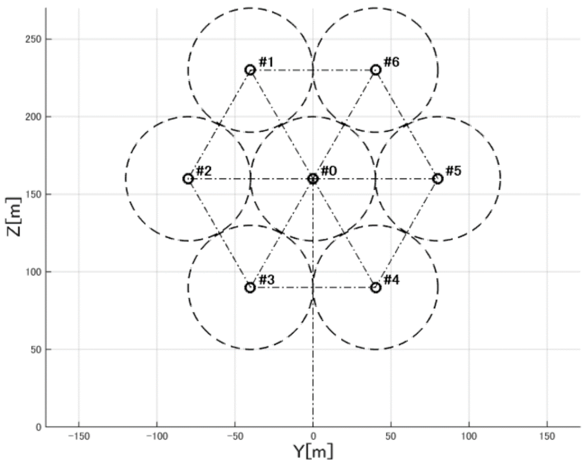

Figure 1. Rotor positions of the 7 × 2 MW MRS.

- The aerodynamic interferences between the support structure and the wind turbine rotors were ignored, as the detailed structure was not designed yet. Additionally, the interactions between the mutual rotors were also ignored, as they provide minor effects on the loads and the performance, as mentioned in [1].

- Elasticities were considered up to the second mode of the blade flapwise and to the first mode of the blade edgewise. Other structures, such as the tower and the nacelle supports, were assumed to be rigid bodies.
- A conventional variable speed, variable pitch control was assumed. The controller parameters were determined based on those used in Yoshida [9].

2.3. Wind Model

- Wind model domain and resolution: Table 2.
- Average wind speed: 4–24 m/s (each 2 m/s).
- Turbulence: Category C (12% at 15 m/s).
- Turbulence model: Kaimal.
- Average wind shear exponent: 0.14.
- Average inclination: 0°.
- Average yaw angle: 0°.
- Coherence decay constant (Equation (2)): 6, 12, 24.

Table 2. Wind model domain and resolution.

Direction	x-wise	y-wise	z-wise
Domain	600 s	300 m	300 m
Resolution	0.05 s	10 m	10 m

The coherence model of the IEC61400-1 [10] was used in this study. As seen from the equation, as the decay coefficient increases, the spatial correlation decreases. Although the IEC designates the decay constant for the SRS to be C = 12, Saranyasoontorn et al. [11] measured a wide range of decay constants from 6 to 24. After consideration, three decay constants were assumed in this study.

$$Coh\,(r,f) = \exp\left[-C\left\{\left(\frac{fr}{V_{hub}}\right)^2 + \left(\frac{0.12r}{L_C}\right)^2\right\}^{\frac{1}{2}}\right] \tag{2}$$

where f is frequency; r is relative distance; V_{hub} is hub wind speed; L_C is coherence scale parameter; and C is coherence decay constant (C = 12 in IEC [9]).

The turbulence intensities of the seven rotor centres are shown in Figure 2. The x-axis is the average wind speed at the centre hub. While these speeds depend on the hub height of each rotor, due to the wind shear, the decay coefficient does not affect them.

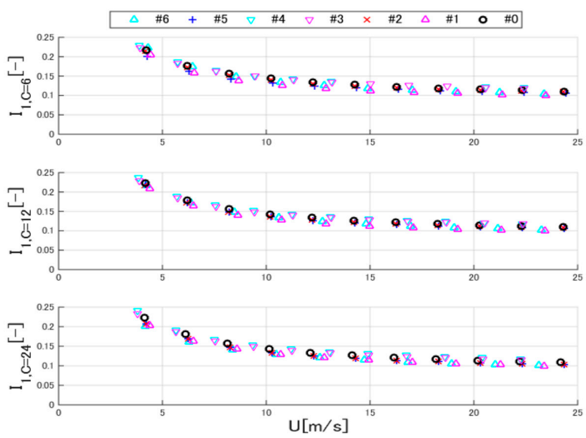

Figure 2. Longitudinal turbulence intensity to wind speed at each hub centre.

The power spectral densities (PSDs) of the wind speed at Rotors #1–#6 are shown in Figure 3. Neither the decay constants nor the turbulence intensities affected the PSDs.

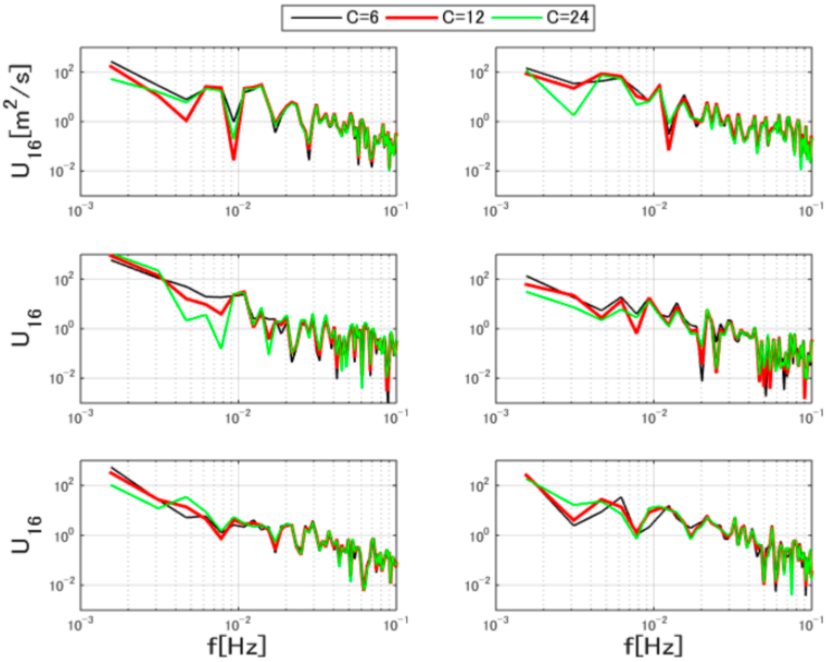

Figure 3. Example of power spectral densities (PSDs) of the longitudinal wind speed at the #1–#6 hub centres (16 m/s).

Figure 4 shows an example of the coherence at 16 m/s and 80 m, which corresponds to the distance between the rotors in the present model. A smaller decay constant shows a larger coherence in the low frequency range and indicates a stronger coherence. As shown in the figure, the coherence changes drastically between 10^{-3} Hz and 10^{-1} Hz, and a larger coherence constant generally provides a smaller coherence.

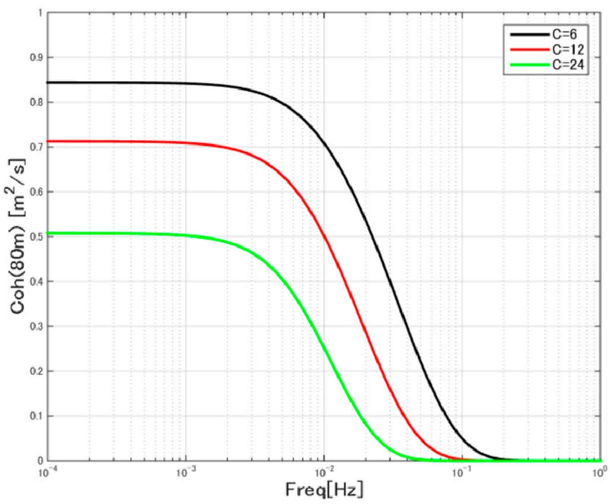

Figure 4. Example of the coherence of the longitudinal wind speed (80 m, 16 m/s).

Figure 5 shows examples of the time histories of the longitudinal wind speed U and yaw angle ψ at each rotor position for a 16 m/s average wind speed. The figure shows that the wind speed is more scattered for a larger decay constant.

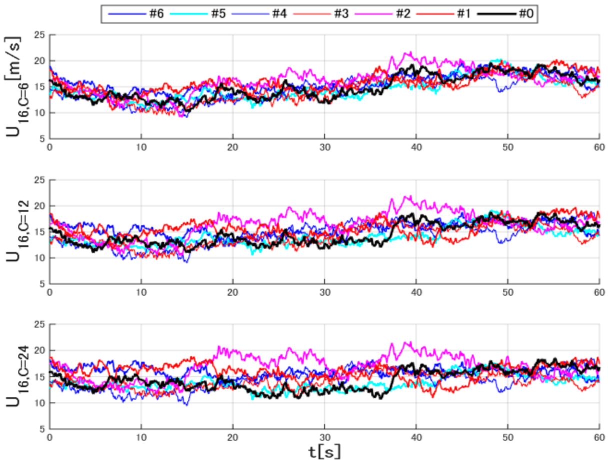

(**a**)

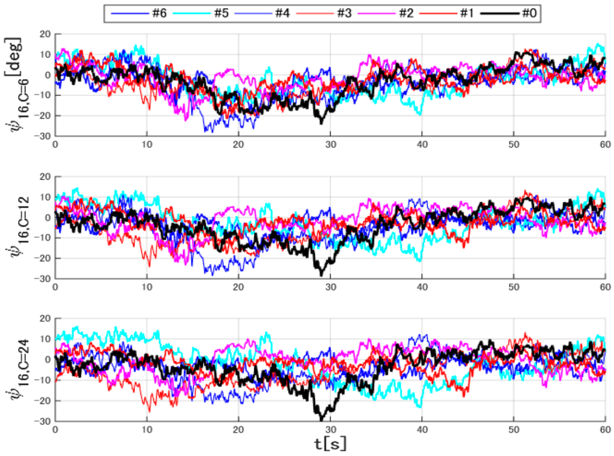

(**b**)

Figure 5. Example of the time history of the wind at the hub centre of each rotor (16 m/s at the centre hub, 0–60 s): (**a**) wind speed and (**b**) yaw angle.

Figure 6 shows examples of the time histories of the standard deviations of the longitudinal wind speed U and yaw angle ψ at each rotor position. Mutual deviations are larger for a larger decay constant, as indicated by Equation (2).

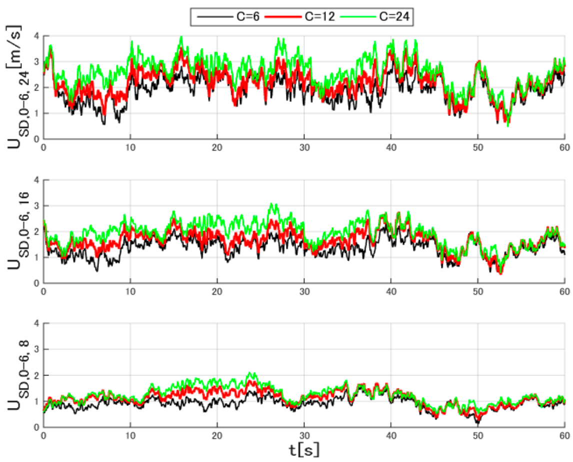

(**a**)

Figure 6. *Cont.*

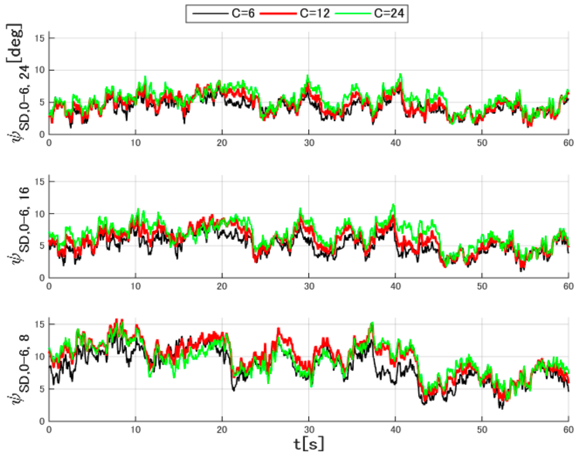

(**b**)

Figure 6. Example of the time history of the standard deviation of seven wind turbines (16 m/s at the centre rotor, 0–60 s): (**a**) wind speed and (**b**) yaw angle.

Figure 7 shows the time-averaged standard deviations of the seven rotors to the average wind speed at the centre hub. This figure also shows that larger decay constants increase the standard deviation. Furthermore, this effect becomes larger as wind speed increases.

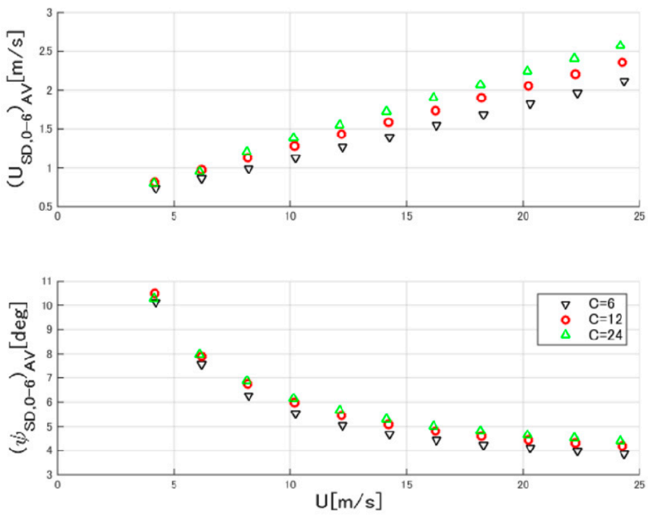

Figure 7. Average of the standard deviations of the wind speed and the yaw angle of seven wind turbines to the average wind speed at the centre hub.

2.4. Analysis Conditions

- Duration: 600 s/case.
- Sampling period: 0.04 s.

3. Basic Characteristics

3.1. Rotor Speed and Pitch Angle

The time-averaged mean and standard deviation of the rotor speed and pitch angle of seven turbines are shown in Figures 8 and 9, respectively. The *x*-axes are the average wind speed at the centre hub.

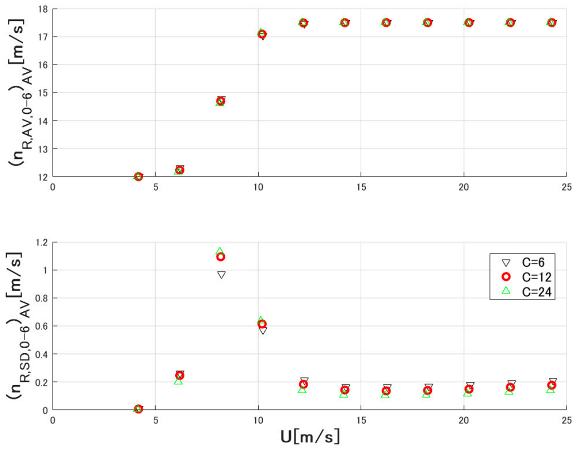

Figure 8. Mean and standard deviation for the rotor speeds of the seven rotors to the average centre hub wind.

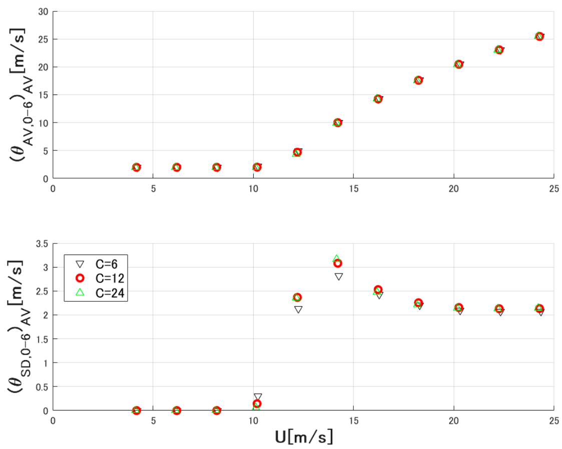

Figure 9. Mean and standard deviation of the pitch angle to the average centre hub wind speed.

The characteristics of the averaged ones are quite common to the variable speed turbines, and the effects of the decay constant are minor. Under low wind speed conditions, the pitch angle and tip speed ratio are maintained under the optimum conditions, whereas the blade pitch controls the rotor speed under high wind speed conditions. The standard deviation of the rotor speed has a peak value of approximately 8 m/s at the high end of the variable speed optimal mode. The standard deviation of the blade pitch angle takes a peak value around the rated wind speeds of 12–14 m/s, where the rotational damping is lower and the rotor speed is sensitive to the wind speed.

3.2. Output Power

Examples of the time histories of the MRS output power are shown in Figure 10. These results are to be expected from the wind coherence. The decay constant does not affect the characteristics at 24 m/s, where the wind turbines operate as rated. However, the decay constant significantly affects the characteristics at 8 m/s. At the high end of the optimal mode operation, the turbine operates at approximately the optimum tip-speed ratio. The output power of an individual turbine approximately varies with the cube of the wind speed. Therefore, the wind coherence affects the characteristics drastically. A slight effect of the decay constant can be seen in the example at 16 m/s. Although there are no differences in the operation at the rated wind speeds, once the wind speeds drop below the rated level, a larger decay constant results in a shallower drop. In conclusion, a larger decay constant results in a smaller power fluctuation.

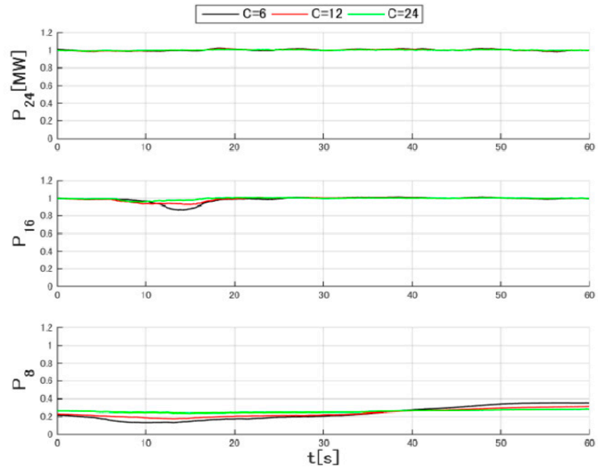

Figure 10. Example of the time history of the total power to the coherence decay constant (24 m/s, 16 m/s and 8 m/s at the centre hub from top to bottom).

The time average of the average and standard deviation of output power of seven turbines is shown in Figure 11. Although no significant differences are found for the average power, the decay constant shows an effect on the standard deviation. A larger decay constant results in a smaller standard deviation in the output power.

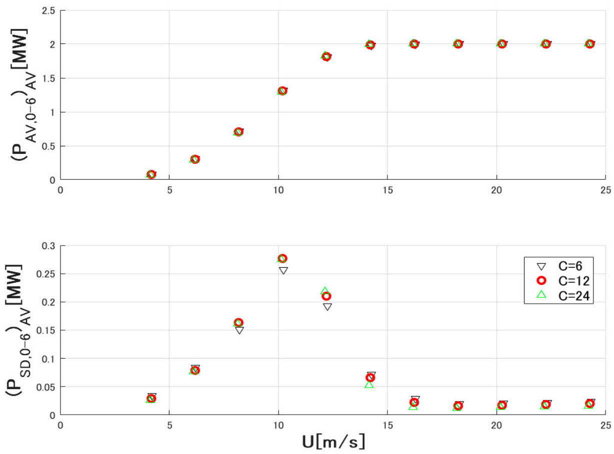

Figure 11. Mean and standard deviation of the output power to the average centre hub wind speed.

4. Tower Loads

Three representative tower loads were investigated in this section. Tower base fore-aft bending is considered a collective load, as it is calculated by the summation of the seven rotors in the same direction. On the other hand, tower top nodding and yawing are considered differential loads, as they are calculated by summation in counter directions.

4.1. Time History

Examples of the time history of the tower base fore-aft bending are shown in Figure 12a. While the graph of the load at 8 m/s is quite similar to that of the output power, this characteristic is maintained in the above rated higher wind speed, unlike the output power, which was maintained at an almost constant rate.

The effects of the differential loads from the tower top nodding and yawing are shown in Figure 12b,c. Although the decay constant affects the loads, the effects are less remarkable than those of the tower base fore-aft bending (a collective load). Some of the peak values from large fluctuations disappeared, although the high-frequency fluctuations increased.

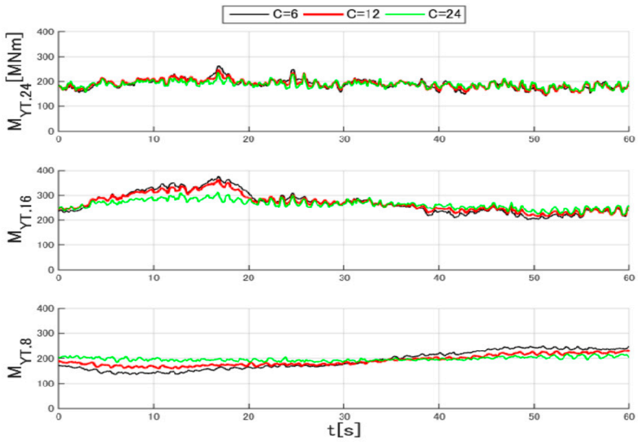

(**a**)

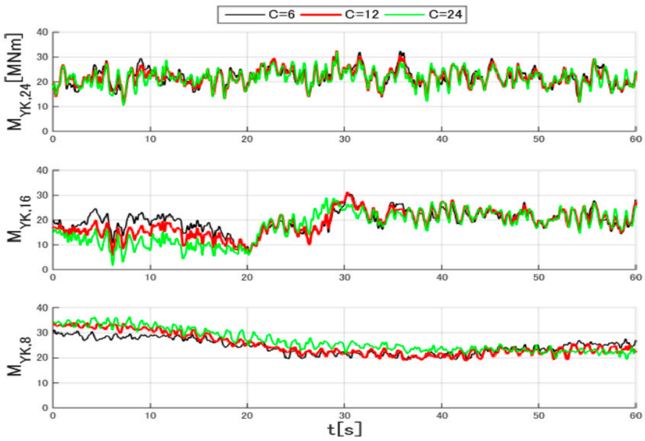

(**b**)

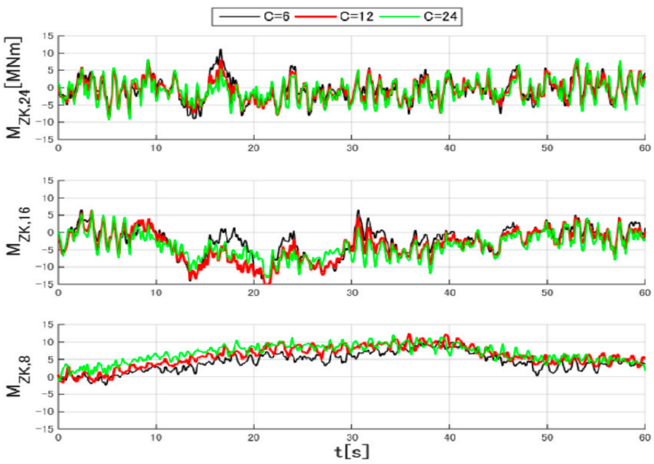

(**c**)

Figure 12. Time history of tower loads (24 m/s, 16 m/s and 8 m/s at the centre hub, 0–60 s): (**a**) tower base fore-aft bending moment; (**b**) tower top nodding moment; and (**c**) tower top yawing moment.

4.2. Statistics to Average Wind Speed

The average and standard deviation of the tower base fore-aft bending is shown in Figure 13a. Larger standard deviations result from the large decay constant in any wind speed range.

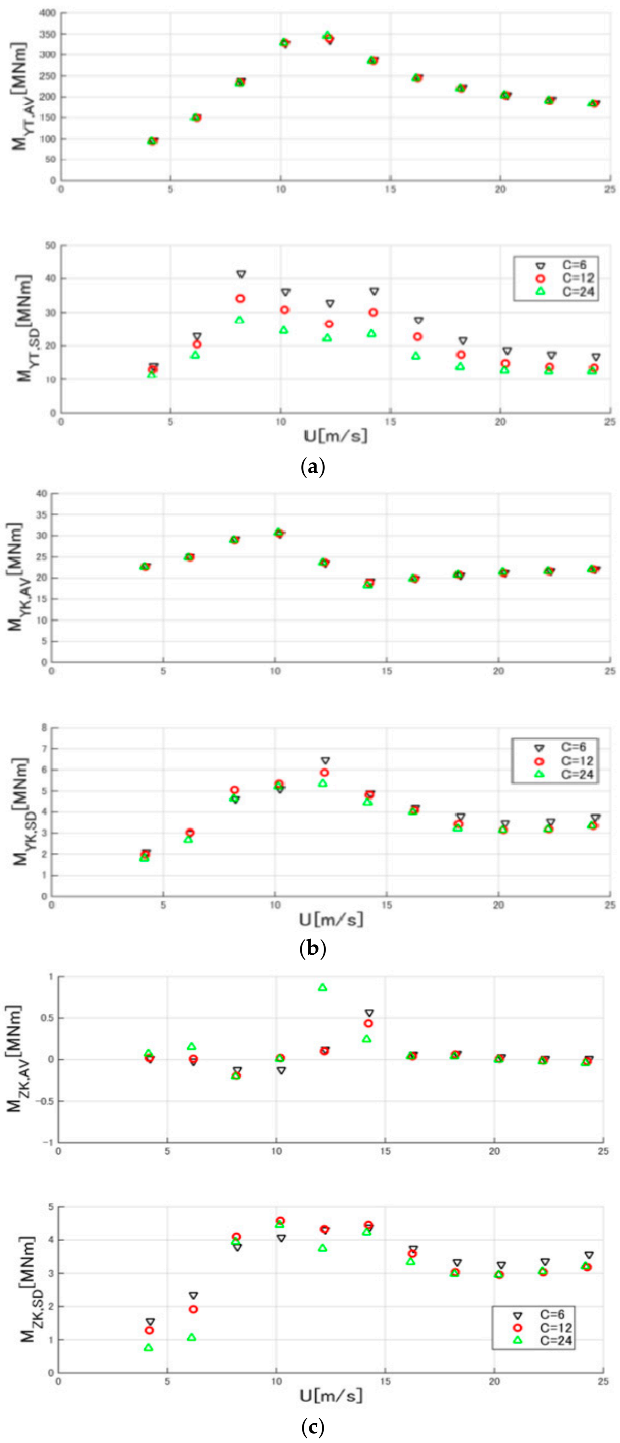

Figure 13. Mean and standard deviation of the tower loads to the average wind speed at the centre hub: (**a**) tower base fore-aft bending moment; (**b**) tower top nodding moment; and (**c**) tower top yawing moment.

The average and standard deviation of the tower top nodding and yawing are shown in Figure 13b,c. As indicated by the time history data, these standard deviations are not as remarkable as those of the tower base fore-aft bending. Larger standard deviations resulted from smaller decay constants in the higher and lower wind speed ranges, whereas larger standard deviations resulted from larger decay constants in the rated wind speed range.

4.3. Power Spectral Density

PSDs of the tower loads are shown in Figure 14. Common to all loads, a larger decay constant provides a lower PSD in the low frequency range. On the contrary, in the high frequency range, the decay constant does not affect the tower base fore-aft bending, although a higher decay constant increases the frequency component by approximately 0.03 Hz.

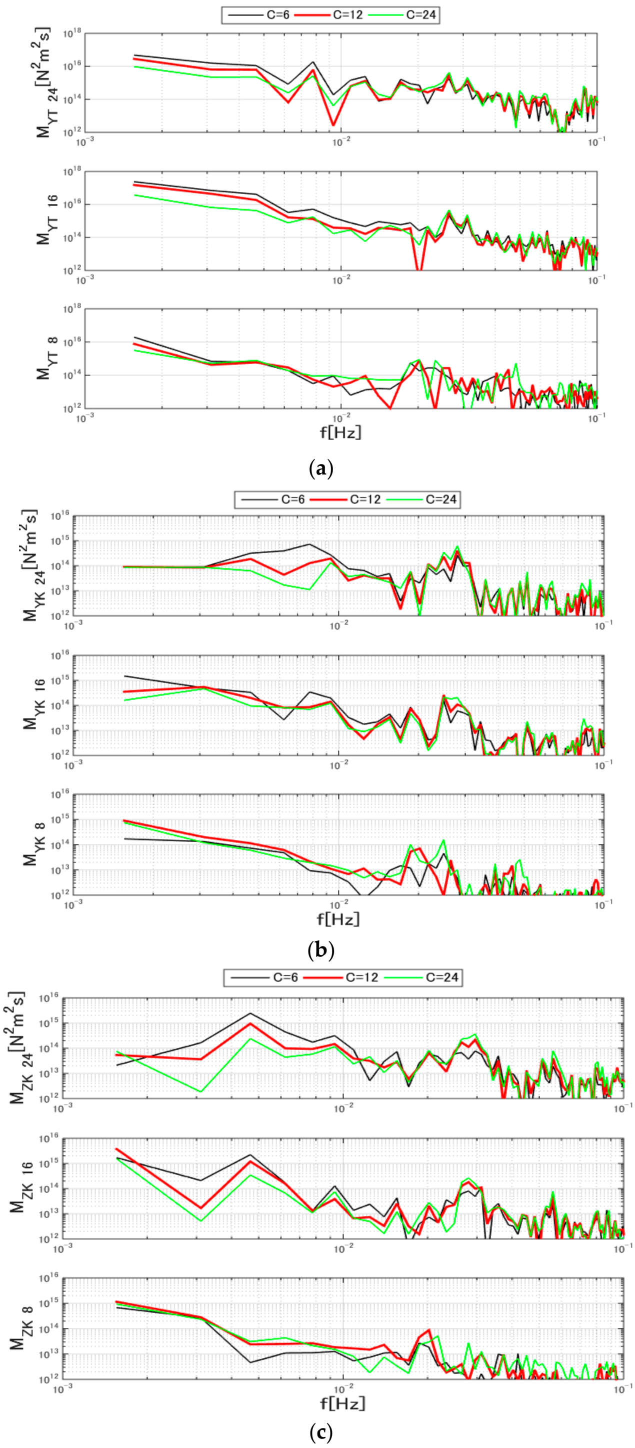

Figure 14. PSD of the tower loads (24 m/s, 16 m/s and 8 m/s from top to bottom): (**a**) tower base fore-aft bending; (**b**) tower top nodding; and (**c**) tower top yawing.

4.4. Fatigue Loads and Damages

This section discusses the fatigue loads and fatigue damages that are more useful in understanding the effects of the decay constant than the other data shown in the previous sections.

Relative damage equivalent loads (DELs) and fatigue damage to the decay constant are shown in Figure 15. An annual average wind speed of 8.5 m/s and an $m = 4$ inverse slope of an S-N curve were assumed here. Both of them are normalized by a decay constant of $C = 12$.

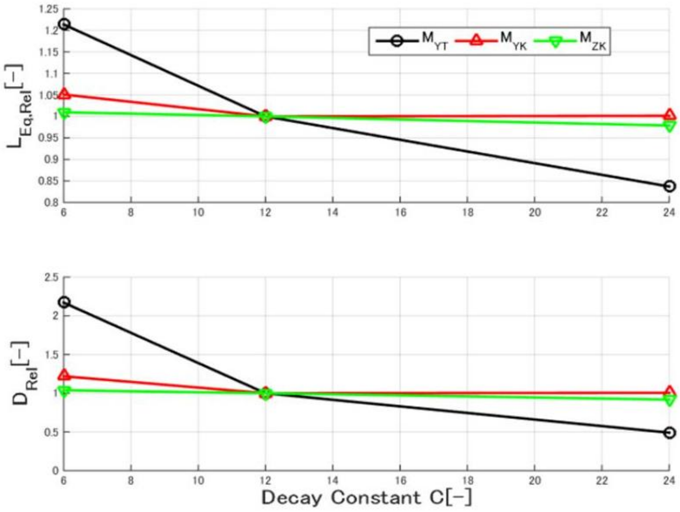

Figure 15. Damage equivalent load (DEL) and relative fatigue damage (8.5 m/s of annual average wind speed, m = 4).

By a comparison between the collective (tower base fore-aft bending) and differential (tower top nodding and yawing) loads, the characteristics of the decay constant are completely different. As the decay constant increases, the damages in the collective loads increase, whereas the damage in the differential loads decreases. In particular, the damage from tower base fore-aft bending fatigue is more than doubled from C = 12 to $C = 6$. This result indicates the risks in designing a large-scale MRSs based on the default parameters in the design standard.

Distributions of the DEL and fatigue damage from tower base fore-aft bending are shown in Figure 16a. This figure shows that the decay constant affects the loads around the rated wind speed drastically. On the contrary, the DEL and fatigue damage of tower top nodding and yawing are increased as the decay constant is increased, as shown in Figure 16b,c.

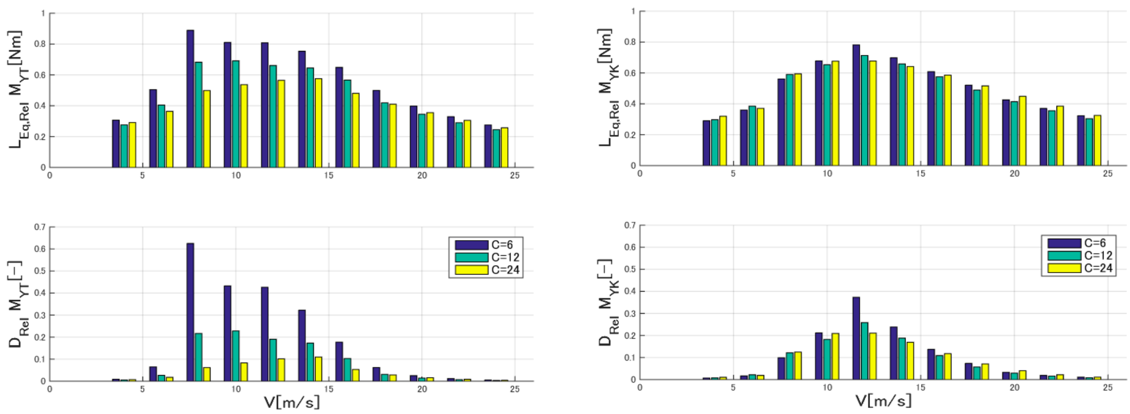

(**a**) (**b**)

Figure 16. *Cont.*

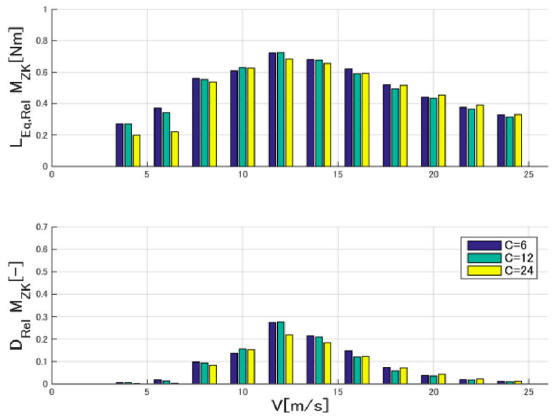

(**c**)

Figure 16. Relative DEL and fatigue damage from the tower loads with $C = 12$ (8.5 m/s of the annual average wind speed, $m = 4$): (**a**) tower base fore-aft bending moment; (**b**) tower top nodding moment; and (**c**) tower top yawing moment.

The rain-flow cycle counts of the tower base fore-aft bending at an 8.5 m/s annual average wind speed are shown in Figure 17a. The numbers of cycles in the large load range are larger for a larger decay constant, although there is an increase in the middle load range.

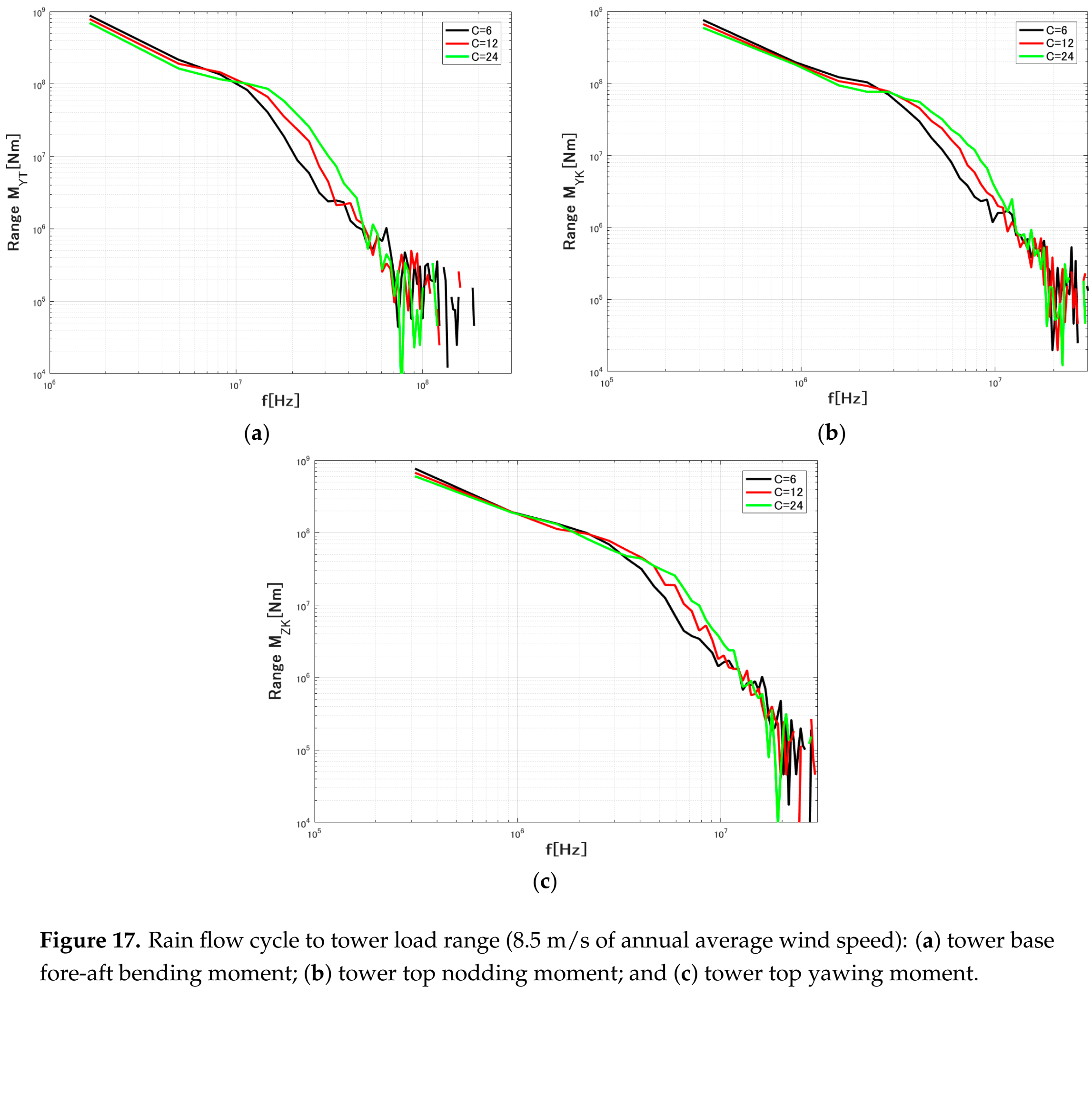

Figure 17. Rain flow cycle to tower load range (8.5 m/s of annual average wind speed): (**a**) tower base fore-aft bending moment; (**b**) tower top nodding moment; and (**c**) tower top yawing moment.

5. Conclusions

- The following results were found through a dynamic simulation of a 7 × 2 MW MRS in this study. The coherence affects the fatigue loads of a large-scale MRS. In the most significant case, the fatigue damage of the tower base fore-aft bending was more than doubled between C = 6 and C = 12.
- The effects of the coherence are different between the collective (tower base fore-aft bending, power, etc.) and differential (tower top nodding, yawing, etc.) loads. A larger coherence causes larger fatigue damages for the collective loads. On the contrary, a smaller coherence causes larger fatigue damages for the differential loads.
- Although an MRS is out of scope of the present IEC61400-1 standard, the coherence should be defined carefully in the design of large-scale MRSs, as it affects the design significantly.

The effects of the decay constant shown here depend on the size and numbers of turbines in the MRS.

The present analyses were carried out ignoring the elasticity of the support structure. The aerodynamic interactions between rotors and support structures were also ignored. Those models are planned to be improved in the future study. Furthermore, statistical reliability will also be investigated, through a number of simulations in different sets of conditions.

Acknowledgments: A part of this study was conducted with funding from the "Research on Over 10 MW Class Wind Turbine Project" of New Energy and Industrial Technology Development Organization (NEDO) in 2013–2014 by contract with HITACHI, Ltd.

Author Contributions: Shigeo Yoshida did most part of the work for the modelling, analyses, discussion and writing of the manuscript. Uli Goltenbott contributed to summarizing the former studies. Yuji Ohya reviewed the wind model and performance. Peter Jamieson provided general and fundamental information for MRS.

Conflicts of Interest: The authors declare no conflict of interest.

Abbreviations

DEL	Damage equivalent load
IEC	International Electrotechnical Commission
MRS	Multi-rotor system
NEDO	New Energy and Industrial Technology Development Organization
PSD	Power spectral density
SRS	Single-rotor system

References

1. Ranson, D.L.; Moore, J.J. *SwRI Engineers Design, Build and Test a Prototype Wind Turbine Array*; Southwest Research Institute: San Antonio, TX, USA, 2009.
2. Goltenbott, U.; Karasudani, T.; Ohya, Y.; Jamieson, P. Aerodynamic analysis of clustered wind lends turbines. In Proceedings of the 8th International Symposium on the East Asian Environment Problems, Fukuoka, Japan, 9–10 December 2014.
3. Jamieson, P. *Multi Rotor Systems, in Innovation in Wind Turbine Technology*; Wiley-Blackwell: Chichester, UK, 2011.
4. Jamieson, P.; Branney, M. Structural considerations of a 20 MW multi-rotor wind energy system. *J. Phys. Conf. Ser.* **2014**, *555*. [CrossRef]
5. Jamieson, P.; Branney, M.; Hart, K.; Chaviaropoulos, P.K.; Sieros, G.; Voustinas, S.; Chasapogiannis, P.; Prospathopoulos, J.M. Deliverable 1.33 Innovative Wind Turbine Concepts—Multi-Rotor System. Available online: http://www.innwind.eu/Publications/Deliverable-reports (accessed on 10 June 2016).
6. Verma, P. Multi Rotor Wind Turbine Design and Cost Scaling. Master's Thesis, University of Massachusetts Amherst, Amherst, MA, USA, September 2013.
7. Mate, G.M. Development of Support Structure for Multi-Rotor Wind Turbines. Master's Thesis, University of Massachusetts Amherst, Amherst, MA, USA, September 2014.
8. *DNV GL, BLADED*, version 4.7; DNV GL: Bristol, UK, 2015.

9. Yoshida, S. Variable speed-variable pitch controllers for aero-servo-elastic simulations of wind turbine support structures. *J. Fluid Sci. Technol.* **2011**, *6*, 300–312. [CrossRef]
10. *Wind Turbines—Part 1: Design Requirements*IEC-61400-1, 3rd ed.; International Electrotechnical Commission: Geneva, Switzerland, 2005.
11. Saranyasoontorn, K.; Manuel, L.; Veers, P.S. A comparison of standard coherence models for inflow turbulence with estimates from field measurements. *J. Sol. Energy Eng.* **2004**, *126*, 1069–1082. [CrossRef]